Spectrum of Engineering Sciences
ISSN (e) 3007-3138 (p) 3007-312X Volume 4, Issue 3, 2026

APPLICATION OF HYBRID MULTI-OBJECTIVE GRAVITATIONAL SEARCH ALGORITHM FOR PROCESS OPTIMIZATION OF CARBON FIBRE-REINFORCED POLYMER

Fareed Ahmad[1], Sahar Noor[*2], Mohammad Abas[3], Syed Haris Iftikhar[4], Abdul Rehman Ahmad[5]

[1,4]*Department of Mechanical Engineering, College of Electrical and Mechanical Engineering, National University of Sciences and Technology, Islamabad, Pakistan*
[*2,3]*Industrial Engineering Dept, University of Engineering and Technology, Peshawar, Pakistan*
[5]*Biomedical Engineering Dept, Ripha International University Islamabad, Pakistan*

[*2]sahar@uetpeshawar.edu.pk

DOI: https://doi.org/10.5281/zenodo.19274180

Keywords
carbon fibre-reinforced polymer (CFRP), optimization, hybrid multi-objective Gravitational Search Algorithm (HMOGSA), Genetic Algorithm

Article History
Received: 28 January 2026
Accepted: 11 March 2026
Published: 28 March 2026

Corresponding Author: *
Sahar Noor

Abstract

This research explores the optimization of carbon fibre-reinforced plastic (CFRP) laminates for aerospace applications, specifically targeting the skin of a medium-format fighter aircraft. The study focuses on modifying the original equipment manufacturer (OEM) general-purpose curing cycle to enhance the mechanical properties of CFRP laminates. Through experimental work, an optimized curing cycle is developed, resulting in superior tensile strength, impact toughness, and hardness of the CFRP laminate. Initially, a single objective Gravitational Search Algorithm (GSA) is employed to validate individual optimum properties of the CFRP laminate. Subsequently, an indigenous Hybrid Multi-objective GSA (HMOGSA) is devised and utilized to validate the experimental results comprehensively. Moreover, to authenticate the findings of the developed HMOGSA, the experimental results are cross-validated using a multi-objective Genetic Algorithm (MOGA). The research findings highlight the efficacy of the proposed HMOGSA approach in optimizing CFRP laminates for aerospace applications. This stud contributes to advancing the understanding and practical implication of optimizing techniques in the design and fabrication of high performance composite materials for aerospace engineering.

1. INTRODUCTION

Carbon fibre-reinforced polymers (CFRPs), represent a class of advanced materials renowned for their exceptional strength, stiffness, and lightweight properties [1]. Comprising a matrix material, typically a polymer resin, reinforced with carbon fibres, CFRPs find extensive applications across diverse industries including aerospace, automotive, sporting goods, marine, and renewable energy sectors [2–5]. The excellent mechanical properties of CFRPs originated from the combination of two distinct materials namely the high-strength carbon fibres and the lightweight polymer matrix. Carbon fibres, composed of tightly bound carbon atoms in crystalline structure, possess significant tensile strength and stiffness, surpassing traditional materials such as steel and aluminium [6,7]. Additionally, carbon fibres exhibit low thermal expansion, excellent corrosion resistance, and superior fatigue properties, making them ideal for demanding engineering applications [8].

The manufacturing process of CFRPs, typically involves several stages, including fibre reinforcement, resin impregnation, and curing [1]. Various techniques and processes such as

automated processes, filament winding, hand layup, resin transfer moulding (RTM) or automated fibre placement (AFP) are employed to achieve delicate control of resin distribution and fibre-orientation, ensuring optimum mechanical properties tailored to specific applications [9].

Optimizing the curing parameters of CFRPs is crucial for achieving high-quality composite materials with desired mechanical properties while minimizing manufacturing costs and cycle times [10]. Key parameters include curing temperature, duration, pressure, resin type and formulation, fibre orientation, layup configuration, and post-cure treatments [11]. Balancing factors like temperature and time ensures complete resin polymerization without thermal damage or excessive cycle times. Pressure aids in void elimination and resin consolidation [12]. Resin type selection and formulation adjustments optimize curing behaviour [13]. Fibre orientation and layup configuration influence mechanical properties and waste reduction [14]. Post-cure treatments can further enhance properties [15].

Lately, the use of nature-inspired algorithms for validation of experimental results has increased. These algorithms have better problem-solving capability, accuracy and consume lesser time than their classical counterparts.

The classical algorithms have limited applicability due to lesser inflexibility [16]. Many researches have highlighted that nature-inspired algorithms conveniently solve complex computational problems including clustering, control functions, pattern recognition, objective functions optimization, classification, filter modelling, and image processing [17,18]. In the last decade many nature-inspired algorithms have been developed such as Particle Swarm Optimization (PSO), Ant Colony Optimization (ACO), Genetic Algorithm (GA), Simulated Annealing (SA), Artificial Bee Colony (ABC), and Big Bang Big Crunch (BB-BC) optimization etc.

GSA is a heuristic optimization method, which was introduced in 2009 by Rashedi et al. [19] to solve optimization problems. This nature-inspired algorithm utilizes the law of gravity and mass interactions. More than 38 versions of GSA have been presented so far by researchers to improve the performance and capability of the original version [20,21]. The initial GSA research paper was a single objective algorithm, which was later hybridized by many researchers to increase its capability and scope to handle complex optimization problems (MOOP). These modified versions have been successfully used to solve engineering problems of route optimization, data clustering, process optimization, optimization of retaining structures, optimization of an industrial flotation column, size optimization of truss structures, and hydraulic turbine governing system parameters identification [16,22,23].

The non-traditional nature-based optimization algorithms have become popular in solving engineering design optimization problems since 1975 [27]. Simulated Annealing and Genetic Algorithms are such two examples, and now GSA is also getting its due share amongst these non-traditional nature-inspired optimization algorithms. capability to escape from local optima, memory-less algorithm, shorter computational time and consistent results [16,22] are the advantages, which make GSA suitable for this study. The use of GSA for finding optimal curing parameters of a composite laminate is novel, as it has not been used for the purpose so far.

In this research work, Pareto dominance is incorporated into multi-objective GSA, which transforms it into a hybrid multi-objective GSA (HMOGSA). The HMOGSA is applied to validate the experimental results of our previous research work [28].

2. Materials and Methods

A prepreg unidirectional carbon fibre-reinforced polymer (UD CFRP) lamina of thickness 0.125 mm was used as sample material in the previous study [28]. Two laminates were prepared with stacking sequences $[0/+45/0/0/0/-45/0]_3$ and $[0/+45/0/0/0/-45/0]_{12}$. The former laminate was used for the fabrication of tensile test coupons whereas the latter was used for impact toughness and harness test coupons.

For the planning of experimentation, a three factor, each comprising of two levels, full factorial DOE was used. ANOVA was used to find significant curing parameters (temperature, time, and autoclave pressure) influencing three responses i.e., tensile strength, impact toughness and hardness of the CFRP laminate. The

laminates were subjected to eight different curing cycles (CCs) as shown in Table A1 (given in annexure) of the previous study [28]. Subsequently, mathematical models were developed to represent relationship between predictors (temperature, time and pressure) and three responses (tensile strength, impact toughness and hardness). The mathematical models are presented as Equations (2), (3) and (4) of previous study [28]. Building on this dataset and mathematical models, the current study aims to validate the experimental data by applying single objective GSA on the mathematical models as objective functions. Later, multi-objective optimization of the two properties (tensile strength and impact toughness) is carried out using indigenous HMOGSA.

3 Gravitational Search Algorithm

GSA is a nature-inspired population-based meta-heuristic algorithm based on Newton's law of gravity. In this algorithm, agents are assumed as objects and their masses are measure of performance[19]. These interacting search agents (masses) follow the Newtonian laws of gravitation and motion. The masses apply gravitational forces on each other which results in mobility of the masses or search agents towards the heaviest mass. The concept is shown in Figure 1. Each solution of the problem is represented by a mass. After every iteration, the masses would be attracted by the larger gravitational force of the largest mass. The better solution is represented by the larger masses, and the largest mass is the optimum solution.

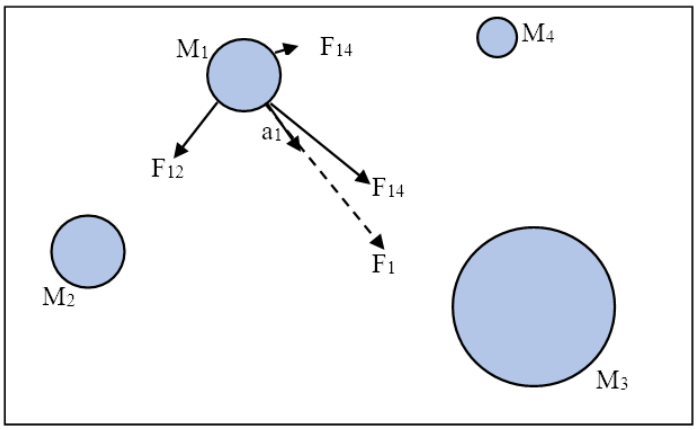

Figure 1. The gravitational force of attraction between masses. The mass M_1 is moving towards the largest mass M_3 with acceleration

The algorithm can be summarized in the following eight steps:

Step 1: Initialization

The first step is an initialization of search agent positions (independent variables) within the decision space, which are randomly generated within the constraints of the problem.

$$X_i = x_i^1, \ldots x_i^d, \ldots x_i^n \quad \text{for i=1,2,.....,N} \tag{1}$$

In our case, there are 24 search agents of tensile strength, impact toughness and hardness, determined in previous study and presented in Table 1. Each search agent depends on three independent variables i.e., temperature time, and autoclave pressure. The position of our three search agents will be represented by Equations 3,4 and 5.

$$TS_i = f_1(X_i); X_i = (T_i, t_i, P_i) \quad for\ i = 1,2,3,\ldots.,24 \tag{2}$$

$$IT_i = f_2(X_i);\ X_i = (T_i, t_i, P_i) \quad for\ i = 1,2,3,\ldots.,24 \tag{3}$$

$$Hd_i = f_3(X_i);\ X_i = (T_i, t_i, P_i) \quad for\ i = 1,2,3,\ldots.,24 \tag{4}$$

where TS is tensile strength, IT is impact toughness, Hd is hardness, X is the position of the search agent, T is temperature, t is time, P is autoclave pressure, n is the number of predictors

or dimensions of decision variable space (temperature, time and pressure), i is counter of search agents, N is the total number of search agents, 24.

The hypothetical relationship between the 24 input variable vectors and the resulting 24 output properties vectors is illustrated in Figure 2. Each input variable vector consists of three dimensions i.e., temperature (T), time (t) and pressure (P). These input variables are related to the properties of the CFRP through Equations (3) to (5).

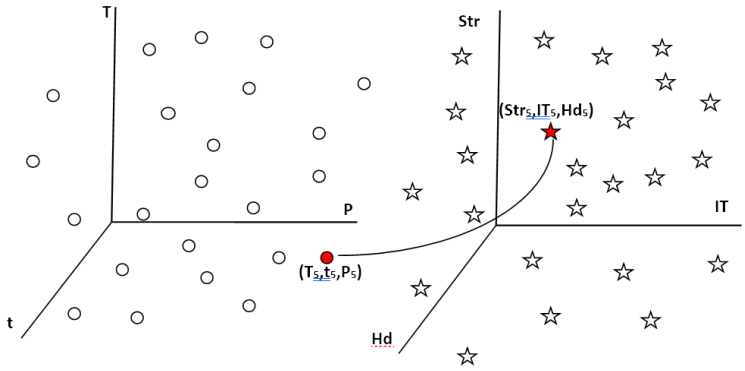

Figure 2. The 24 search agent positions (input variables 'o') and the resulting 24 search agents (output variables/properties ' ') from Equations (3) to (5). The search agent position (T_5,t_5,P_5) is a three dimensional input variable vector corresponding to the search agent (Str_5, IT_5, Hd_5), the properties vector of CFRP

Step 2: Fitness Evaluation

During the fitness evaluation of the objective, the best and worst fitness are computed at each iteration, described mathematically as follows:

$$best(t_n) = \min_{j\in\{1,\ldots,24\}} fit_j(t_n) \quad (5)$$

$$worst(t_n) = \max_{j\in\{1,\ldots,24\}} fit_j(t_n) \quad (6)$$

Where $fit_j(t_n)$ is the fitness of j^{th} agent of iteration t_n, best(t) is the best (min) fitness of all agents, for a minimization problem, worst(t_n) is the worst(max) fitness of all agents, for a minimization problem

Step 3: Computation of Gravitational Constant

The gravitational constant $G(t_n)$ is calculated at iteration t_n in this step as follows:

$$G(t_n) = G_o e^{-\alpha \frac{t_n}{T_n}} \quad (7)$$

Where, G_o is the randomly selected initial value of the constant, α is a constant, T_n is the total number of iterations.

Step 4: Update of Masses

After each iteration, the gravitational and inertial masses are updated for each agent at iteration as follows:
$M_{ai}=M_{pi}=M_{ii}=M_i$, i=1,2,.....,24

$$m(t_n) = \frac{fit(t_n) - worst(t_n)}{best(t_n) - worst(t_n)} \quad (8)$$

$$M_i(t_n) = \frac{m_i(t_n)}{\sum_{j=1}^{24} m_i(t_n)} \quad (9)$$

Where M_{ai} and M_{pi} are is the active and passive mass of the i^{th} agent respectively, M_{ii} is the inertia mass of the i^{th} agent, $M_i(t_n)$ is the mass of the i^{th} agent at iteration t_n.

Step 5: Total Force Calculation

The total force acting on the i^{th} agent is calculated as follows:

$$F_i^3(t_n) = \sum_{j \in kbest, j \neq i} rand_j F_{ij}^3(t_n) \quad (10)$$

Where $rand_j$ is a random number between 0 to 1, kbest is the set of first k agents with the best fitness value and biggest mass

The force acting on the i^{th} mass from the j^{th} mass at iteration t_n is described as follows:

$$F_{ij}^3(t_n) = G(t_n) \frac{M_{pi}(t_n) \times M_{aj}(t_n)}{R_{ij}(t_n) + \varepsilon} (x_j^3(t_n) - x_i^3(t_n)) \quad (11)$$

Where $R_{ij}(t_n)$ is the Euclidian distance between i^{th} and j^{th} agents, ϵ is a small constant

Step 6: Calculation of Velocity and Acceleration

The law of gravity and law of motion is used to calculate the acceleration and velocity of the i^{th} agent at iteration "t_n".

$$a_i^3(t_n) = \frac{F_i^3(t_n)}{M_{ii}(t_n)} \quad (12)$$

$$v_i^3(t_n + 1) = rand_i \times v_i^3(t_n) + a_i^3(t_n) \quad (13)$$

Step 7: Update the Agents' Positions

The subsequent position of the i^{th} agent in the d^{th} dimension is updated as follows:

$$x_i^3(t_n + 1) = x_i^3(t_n) + v_i^3(t_n + 1) \quad (14)$$

Step 8: Repetition

For iterative operation, Section 3.2 to Section 3.7 is repeated until the termination criteria are reached. In the final iteration, the algo returns the position vector of the search agents (input parameters) and the value of the search agent (properties). The steps explained above are presented in a flow diagram, as illustrated below in Figure 2.

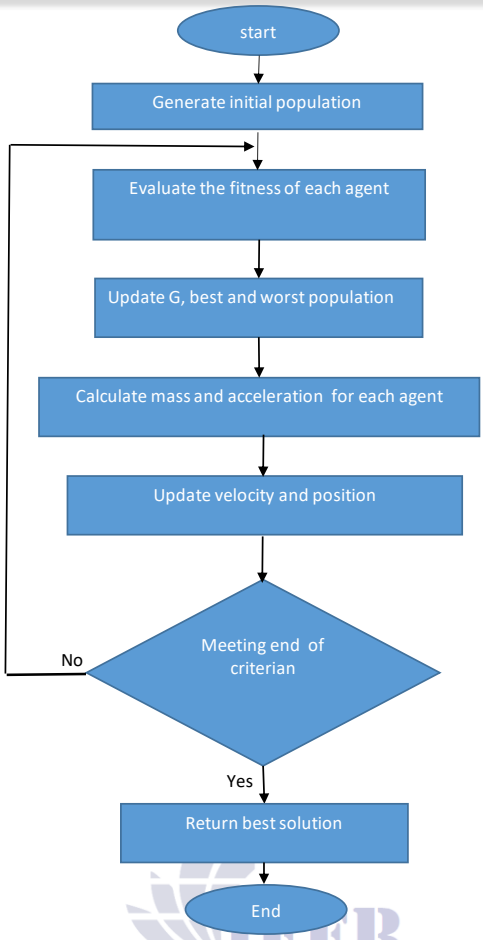

Figure 3. Flow diagram of GSA

4 Multi-objective Optimization

A multi-objective optimization problem (MOOP) is generally defined as shown in Equation (15) [45]

$$min/max\ f_1(x), f_2(x) \ldots . f_n(x) \quad (15)$$
$$subject\ to:\ \ x \in U$$

where; x is a solution of the problem, n is the number of objective functions, U is the feasible solutions set, $f_n(x)$ is nth objective function and min/max is combined object operations

MOOP are solved by researchers by using various techniques. Some of the classical methods used to solve MOOP are Weighted metric, ϵ-constraint, weighted sum, goal programming, value function, interactive and Benson's method. Direct methods and gradient-based methods are the two sub-classes of the classical methods [24]. Direct methods do not use derivative information, whereas gradient-based methods use first and second-order derivative information to reach its destination. A deterministic procedure is used by most of the classical algorithms to reach the optimum solution. These algorithms begin with a pre-specified transition rule random guess solution for the search. The local information/data is exploited during the search. Along the search direction, a unidirectional search is then performed. Till the achievement of the best solution, the iterative procedure is repeated. While using the classical methods certain difficulties are encountered which compelled researchers to develop more advanced evolutionary methods. The difficulties are summarized as follows: -

- The initial randomly chosen solution influences the optimal solution.

- The algorithms are stuck in local suboptimal solutions, an easy trap for most of the algorithms.
- The efficiency of the individual method keeps on according to the optimization problem.
- These algorithms are Inefficient in handling discrete search space.

In a MOOP, there is a function vector for every solution (x) in the decision variable space. A trade-off for the desired solution is therefore required by the decision maker from the available set of solutions [25,26].

5. Results and Discussions

The three properties of CFRP laminate i.e., tensile strength, impact toughness and hardness, optimized by using experimental results (previous study) are summarized in Table 2. In this section, each of the optimized properties is validated using single-objective GSA (SOGSA) individually. The initiating parameters of GSA are presented below:

Number of search agents=24 (experimental results);
Maximum iteration allowed=100;
ElitistCheck=1; R_{power}=1; α=2; G_o=10;

5.1. Single-objective GSA Validation

The SOGSA output is illustrated in Figures 4(a)-(c). The optimum value of tensile strength, impact toughness and hardness were achieved at 56th, 58th and 23rd iteration by SOGSA respectively.

All three graphs exhibit a stepwise increase, indicating the algorithm's iterative convergence towards optimal solutions. It suggests that GSA effectively enhances tensile strength, impact toughness, and hardness. The significant improvements in the early iterations indicate that the algorithm quickly finds near-optimal solutions, while the minor adjustments in later iterations demonstrate its fine-tuning capabilities. The plateaus in the graphs indicate phases where the algorithm thoroughly explores the search space before making further improvements, showcasing its efficiency and robustness in the optimization process.

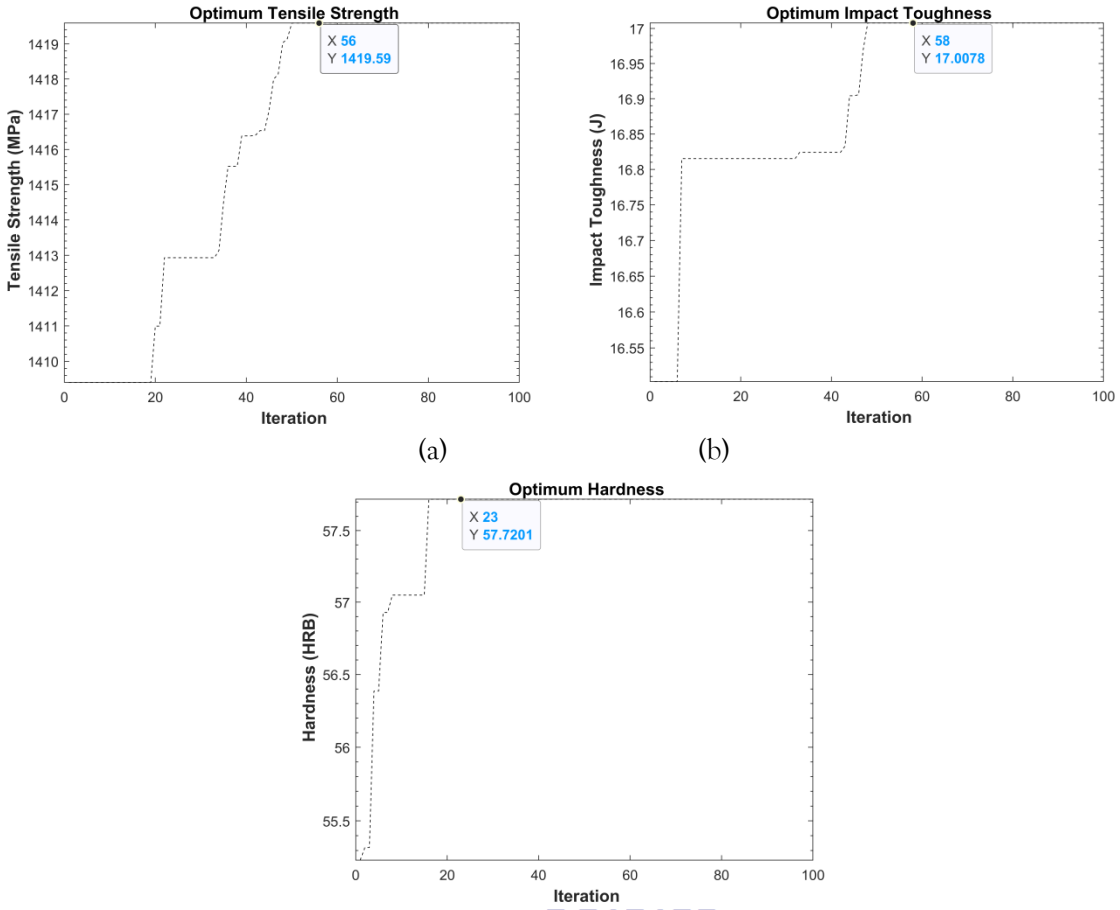

Figure 4. The optimum value of (a) tensile strength (1419.59 MPa) (b) impact toughness (17.00 J) and (c) hardness (57.72 HRB) was achieved on 56th, 58th, and 23rd iteration respectively

The optimum value of tensile strength, impact toughness and hardness determined experimentally in the previous study [28] and the optimized results validated through SOGSA are presented in Tables 3, 4 and 5 respectively for comparison. In terms of tensile strength, as shown in Table 3, the optimal curing cycle parameters i.e., temperature, time, and pressure resulted in experimental values that closely matched the SOGSA results. The experimental tensile strength at 140°C was 1420 MPa, while the SOGSA predicted 1419.59 MPa, leading to a minimal error of 0.0288%. This small discrepancy indicates the robustness of the SOGSA in predicting tensile strength under optimal curing conditions.

Table 3. Comparison of experimental and SOGSA validated results: Tensile Strength

Optimal Curing Cycle				Optimum Property: Tensile Strength		
Curing Parameters	Exp Results	GSA Results	Error (%)	Exp Results	GSA Results	Error (%)
Temperature (°C)	140.0	139.8	0.143			
Time (min)	120.0	119.9	0.083	1420.00	1419.59	0.029
Pressure (bar)	7.0	6.9	1.429			

Similarly, for impact toughness, presented in Table 4, the experimental results and SOGSA predictions were in close alignment. The optimal curing temperature of 140°C yielded an

experimental impact toughness of 17.4 J, compared to the SOGSA result of 17.00 J, resulting in a slightly higher error of 2.298%. While this error is slightly larger than that observed for tensile strength, it still falls within an acceptable range, demonstrating that SOGSA is a reliable method for optimizing impact toughness.

Table 4. Comparison of experimental and SOGSA validated results: Impact Toughness

Optimal Curing Cycle				Optimum Property: Impact Toughness		
Curing Parameters	Exp Results	GSA Results	Error (%)	Exp Results	GSA Results	Error (%)
Temperature (°C)	140.0	139.9	0.143			
Time (min)	120.0	119.6	0.083	17.40	17.00	2.298
Pressure (bar)	3.0	3.2	6.667			

Table 5 details the hardness results, which also show a strong correlation between experimental and SOGSA-predicted values. The hardness of the material at the optimal curing temperature of 140°C was measured experimentally at 57.60, while SOGSA predicted a value of 57.72, resulting in a negligible error of -0.002%. This extremely low error underscores the accuracy of SOGSA in predicting hardness under optimal conditions.

Table 5. Comparison of experimental and SOGSA validated results: Hardness

Optimal Curing Cycle				Optimum Property: Hardness		
Curing Parameters	Exp Results	GSA Results	Error (%)	Exp Results	GSA Results	Error (%)
Temperature (°C)	140.0	139.9	0.143			
Time (min)	120.0	118.7	1.083	57.60	57.72	0.002
Pressure (bar)	7.0	6.9	1.429			

The differences between the experimental and SOGSA results across the three properties i.e., tensile strength, impact toughness, and hardness are minor, with the percentage error ranging from 0.002% to 2.298%. The input variable differences, ranging from 0.083% to 6.667%, indicate that the optimization process using SOGSA is highly effective in predicting the optimal curing cycle parameters. These results validate the use of SOGSA as a reliable and accurate optimization tool for enhancing the mechanical properties of CFRP laminates. The close agreement between experimental and optimized results highlights the potential of SOGSA in industrial applications where precise control of material properties is crucial.

5.2. Hybrid Multi-objective GSA Optimization

Most of the practical engineering problems are multi-objective in nature and therefore require optimization of two or more response parameters. This research also involves validation of the three optimum properties of CFRP i.e., tensile strength, impact toughness and hardness. The results obtained in our previous study (Table 6) [28] show that the optimal curing cycle for tensile strength and hardness was the same (140° C, 120 min, 7 bar). However, the optimal curing cycle for impact toughness was observed to be different (140°C, 120 min, 3 bar). In the existing scenario, there are two possibilities for applying HMOGSA to determine the Pareto Front of the properties i.e., tensile strength vs impact toughness, or hardness vs impact toughness. We selected the former combination for applying HMOGSA in this research paper. The flow diagram of the HMOGSA used in this research work for two objectives is shown in Figure 5.

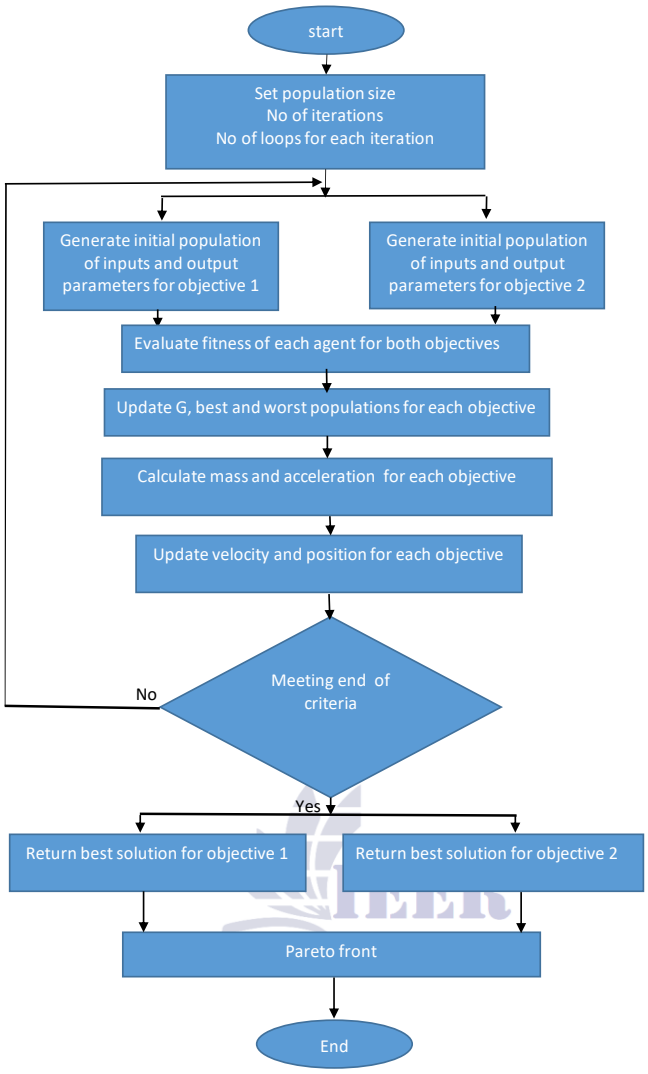

Figure 5. Flow diagram of HMOGSA, for two objectives

The output and optimum properties obtained from HMOGSA are shown in Figure 6. The blue dots on the graph represent the raw output data obtained from the HMOGSA, and their spread indicates the diversity and distribution of solutions generated by the algorithm, crucial for effectively exploring the solution space in multi-objective optimization. The red circles highlight the Pareto optimal solutions, are clustered towards the upper right corner of the graph are the best trade-offs among the objectives in a multi-objective optimization problem. This positioning indicates that these solutions offer the best trade-offs among the objectives being optimized, specifically around tensile strength of 1410 to 1420 MPa and impact strength of 17 to 17.5 J. Due to the multi-objective nature of the problem, there is no unique solution to the problem but a set of non-dominated optimum solutions (Pareto Front) was obtained, a close-up of the Pareto Front is shown in Figure 7 and summarized in Table 6. The identification of these optimal points highlights the algorithm's effectiveness in handling multi-objective optimization problems by finding solutions that balance the trade-offs between conflicting objectives.

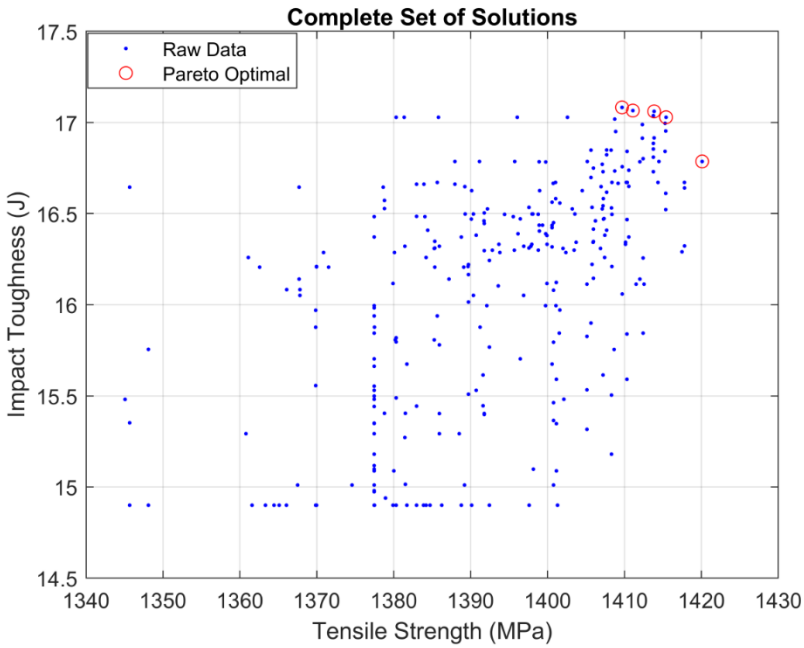

Figure 6. The complete set of solutions. The five nondominated optimum sets (encircled) of solutions accumulated at the right upper corner as Pareto Front

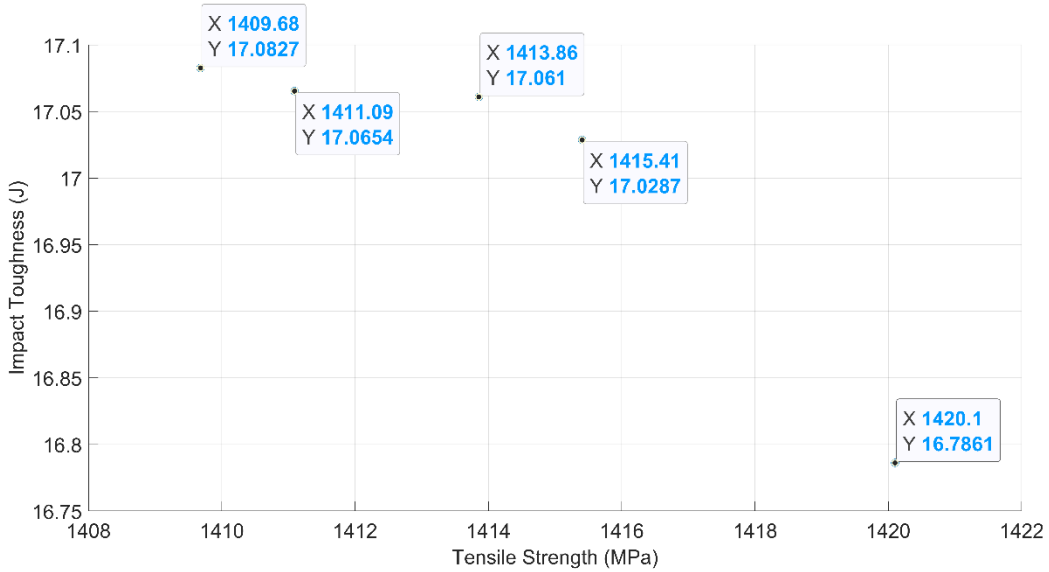

Figure 7. A close-up of the five non-dominated optimum solutions of the multi-objective problem

The Table 7 summarizes five sets of optimal properties alongside their corresponding curing cycles. The first optimal solution features a tensile strength of 1409.68 MPa and an impact toughness of 17.0827 J, achieved with a curing cycle of 139.78°C, 119.45 minutes, and 6.15 bars. The second optimal solution, with a tensile strength of 1411.09 MPa and an impact toughness of 17.0654 J, was obtained using a curing cycle of 139.86°C, 119.58 minutes, and 6.05 bars. Similarly, the third set yields a tensile strength of 1413.86 MPa and an impact toughness of 17.061 J with a curing cycle of 139.85°C, 119.47 minutes, and 6.84 bars. The fourth optimal point achieves 1415.41 MPa tensile strength and 17.0287 J impact toughness, with parameters of 139.57°C, 119.97 minutes, and 6.62 bars. Lastly, the fifth solution has a tensile strength of 1420.10 MPa and impact strength of 16.7861 J, requiring a curing cycle of 139.98°C, 119.98 minutes, and 6.92 bars. These results emphasise the multi-objective nature of

the optimization problem, where single unique solution is not feasible. Instead, a set of non-dominated solutions, or the Pareto Front, is obtained, each representing a different trade-off between tensile strength and impact toughness. Decision-makers can select from these optimal solutions based on specific requirements or preferences, such as prioritizing either tensile strength or impact toughness. The diversity of the Pareto Front provides flexibility, allowing for tailored solutions that best meet the desired performance criteria.

Table 6. Summary of the five sets of optimum properties (tensile strength and impact toughness) and corresponding curing cycles

S No	Optimal Curing Cycles			Non-dominated Optimum Properties	
	Temperature (°C)	Time (min)	Pressure (bar)	Tensile Strength (MPa)	Impact Toughness (J)
1	139.78	119.45	6.15	1409.68	17.08
2	139.86	119.58	6.05	1411.09	17.07
3	139.85	119.47	6.84	1413.86	17.06
4	139.57	119.97	6.62	1415.41	17.03
5	139.98	119.98	6.92	1420.10	16.79

Table 7 compares the optimal curing parameters and properties obtained through both experimental methods and the HMOGSA. This comparison highlights the effectiveness and accuracy of the HMOGSA in predicting optimal outcomes for tensile strength and impact toughness. For tensile strength, the experimental method determined that the optimal curing parameters are temperature of 140.0°C, a time of 120.0 minutes and a pressure of 7.0 bars, yielding an optimum tensile strength of 1420.0 MPa. However, the HMOGSA identified slightly different optimal curing parameters i.e. 139.8°C, 119.5 minutes, and 6.8 bars, resulting in tensile strength of 1413.8 MPa. The difference in optimum tensile strength between the two methods is minimal, with the HMOGSA result being just 0.4% lower than the experimental result. This close agreement demonstrates that the HMOGSA is highly effective in approximating the optimal tensile strength. For impact toughness, the experimental method again used the parameters of 140.0°C, 120.0 minutes, and 7.0 bars, achieving an impact toughness of 16.5 J. The HMOGSA suggested similar parameters (139.8°C, 119.5 minutes, and 6.8 bars) however resulted in higher impact toughness of 17.1J. The difference is 3.6%, including that the HMOGSA predicted slightly higher outcome for impact toughness compared to the experimental method. This difference suggests that the HMOGSA may provide optimized conditions for maximizing impact toughness.

The above comparison demonstrates that the HMOGSA is a reliable tool for predicting optimal curing parameters and resulting properties, closely aligning with experimental results while occasionally even surpassing them. The slight differences in the optimum property values highlights the robustness and precision of the algorithm, making it a valuable approach for multi-objective optimization problems. The ability to predict and optimize these properties can effectively lead to improved performance and efficiency in manufacturing processes.

Table 7. Comparison of optimal curing parameters and optimum properties obtained through experimentation and HMOGSA.

SNo	Determination Mode	Optimal Curing Parameters			Property	Optimum Value	Difference in Optimum Property Value (%)
		Temperature	Time	Pressure			
1	Experimental	140.0	120.0	7.0	Tensile Strength	1420.00 MPa	0.4%
2	HMOGSA	139.8	119.5	6.8	Tensile Strength	1413.86 MPa	
3	Experimental	140.0	120.0	7.0	Impact Toughness	16.5 J	-3.6%
4	HMOGSA	139.8	119.5	6.8	Impact Toughness	17.1 J	

5.3. Comparison of HMOGSA with MOGA Results

The experimental results of our earlier study optimized through RSM [52] are validated through HMOGSA. To revalidate the results of HMOGSA, another very popular algorithm, the multi-objective Genetic Algorithm (MOGA) was used. The Pareto Front obtained through MOGA is shown in Figure 8 and the optimal curing parameters and optimum properties are summarized in Table 8. When equal importance is given to both objective functions, the median values of the result (SNo 9 and 10) are the best compromise.

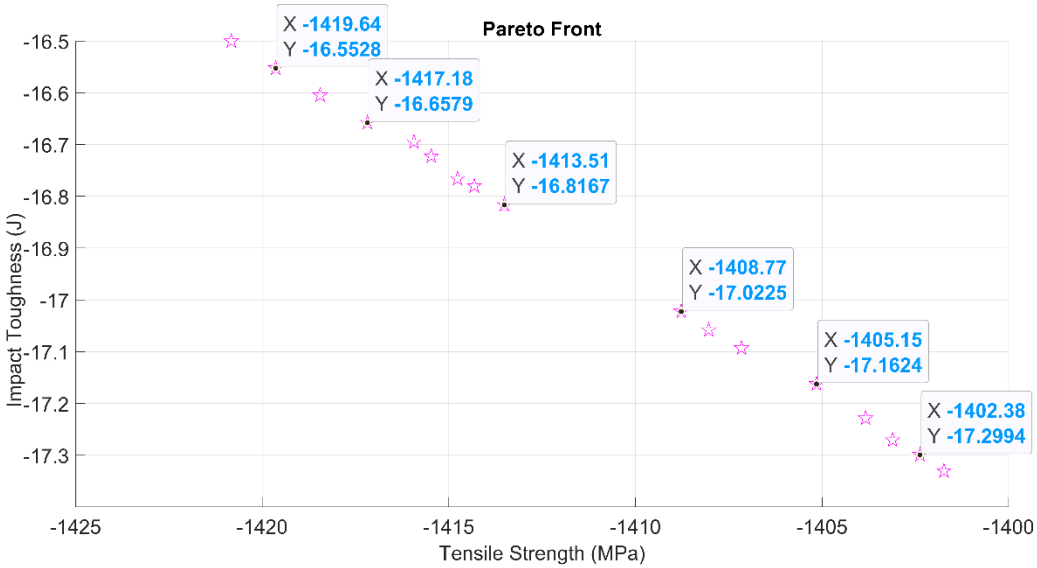

Figure 8. MOGA result for the multi-objective optimization of tensile strength and impact toughness

Table 8 summarizes eighteen sets of optimal properties, including their corresponding curing cycles. For instance, the first optimal solution is achieved with a curing cycle of 139.99°C, 120.00 minutes, and 3.01 bars, resulting in a tensile strength of 1401.73 MPa and an impact toughness of 17.33 J. Similarly, the second solution, using parameters 139.99°C, 120.00 minutes, and 3.15 bars, yields a tensile strength of 1402.38MPa and an impact toughness of 17.30 J. The subsequent solutions demonstrate a range of optimal curing parameters, with corresponding tensile strengths and impact toughness values. As the pressure increases, there is general trend of increasing tensile strength and decreasing impact toughness. For example, the solution with a curing cycle of 139.99°C, 120.00 minutes, and 4.49 bars results

in a tensile strength of 1408.77 MPa and an impact toughness of 17.02 J. Further, along the Pareto Front, at higher pressures such as 7.00 bars, the optimal solutions show tensile strengths of 1420.83 MPa but lower impact toughness of 16.50 J. This shows that the MOGA effectively explores the solution space, offering a comprehensive set of optimal curing cycles and their corresponding properties.

Table 8. Summary of the eighteen sets of optimum properties (tensile strength and impact toughness) and corresponding curing cycles (MOGA)

S No	Optimal Curing Cycles			Non-dominated Optimum Properties	
	Temperature (°C)	Time (min)	Pressure (bar)	Tensile Strength (MPa)	Impact Toughness (J)
1	139.99	120.00	3.01	1401.73	17.33
2	139.99	120.00	3.15	1402.38	17.30
3	139.99	120.00	3.30	1403.11	17.27
4	139.99	119.99	3.47	1403.83	17.23
5	139.98	119.99	3.77	1405.15	17.16
6	139.99	120.00	4.15	1407.16	17.09
7	140.00	120.00	4.32	1408.03	17.06
8	139.99	120.00	4.49	1408.77	17.02
9	139.99	120.00	5.48	1413.51	16.82
10	139.99	120.00	5.65	1414.32	16.78
11	140.00	120.00	5.73	1414.77	16.77
12	139.99	119.99	5.91	1415.47	16.72
13	140.00	119.98	6.02	1415.93	16.70
14	140.00	120.00	6.24	1417.18	16.66
15	140.00	120.00	6.50	1418.45	16.61
16	140.00	120.00	6.75	1419.64	16.55
17	140.00	120.00	7.00	1420.83	16.50
18	140.00	120.00	7.00	1420.83	16.50

The comparison of the optimum properties validated through the HMOGSA and the MOGA is summarized in Table 9. It presents the results of a two-sample t-test to evaluate the null hypothesis, as stated in Equation 16, which posits that there is no significant difference between the means of the optimal results obtained by the two algorithms. The alternate hypothesis, shown in Equation 17, suggests that there is a significant difference between the means.

Null Hypothesis $H_0 = \mu_1 - \mu_2 = 0$ (16)

Alternate Hypothesis $H_a = \mu_1 - \mu_2 \neq 0$ (17)

The results for tensile strength and impact toughness, as obtained through both HMOGSA and MOGA, were analysed to test the null hypothesis. For tensile strength, the HMOGSA algorithm produced a mean value of 1414.03 MPa with a standard deviation of 4.07, based on 5 samples. The MOGA algorithm resulted in a slightly lower mean tensile strength of 1411.73 MPa, with a higher standard deviation of 6.71, across 18 samples. The standard errors of the means were 1.8 for HMOGSA and 1.6 for MOGA. The t-test for tensile strength yielded a t-value of 0.72 with 21 degrees of freedom and a P-value of 0.477. Since the P-value is greater than 0.05, it indicates that there is no significant difference between the tensile strength results of the two optimization algorithms, thus supporting the null hypothesis.

For impact toughness, the HMOGSA algorithm achieved a mean value of 17.00 J with a standard deviation of 0.12, while the MOGA algorithm reported a slightly lower mean impact toughness

of 16.89 J with a standard deviation of 0.29. The standard errors of the means were 0.05 for HMOGSA and 0.07 for MOGA. The t-test value for impact toughness is 0.84 with 21 degrees of freedom and a P-value of 0.41. Similar to the tensile strength results, the P-value being greater than 0.05 indicates no significant difference between the impact toughness results from the two algorithms, further supporting the null hypothesis.

In conclusion, the two-sample t-test results indicate that the differences in the optimal tensile strength and impact toughness values obtained through HMOGSA and MOGA are not statistically significant. The P-values of 0.477 for tensile strength and 0.41 for impact toughness are both above the 0.05 threshold, affirming that the null hypothesis is valid. Therefore, it can be inferred that both optimization algorithms, HMOGSA and MOGA, are equally effective in achieving optimal results for tensile strength and impact toughness in the context of this multi-objective optimization problem. This validation provides confidence in the use of either algorithm for similar optimization tasks in material science and engineering applications.

Table 9. A two-sample t-test results. The P-value is greater than 0.05, which shows that the results are not significantly different.

SNo	Sample	Optimization Algo	N	Mean	Std Dev	SE Mean	T-value	DF	P-value
1	Tensile Strength	HMOGSA	5	1414.03	4.07	1.8	0.72	21	0.477
2	Tensile Strength	MOGA	18	1411.73	6.71	1.6			
3	Impact Toughness	HMOGSA	5	17.00	0.12	0.05	0.84	21	0.41
4	Impact Toughness	MOGA	18	16.89	0.29	0.07			

6. Conclusions

(a) The optimum values of tensile strength, impact toughness, hardness and the corresponding optimal curing cycle determined through SOGSA, and HMOGSA validates the experimental values obtained in previous research work.

(b) The HMOGSA results are also revalidated through MOGA results. No significant difference was observed in the results achieved either through HMOGSA or MOGA.

Disclosure statement

The authors report there are no competing interests to declare.

Data availability statement

All the data is available in the manuscript.

Appendix

Table A1. 2^3 full factorial design and mechanical tests results. MRCC parameters and corresponding properties are represented by bold numbers [28]

Curing Cycle	Temperature (°C)	Time (min)	Pressure (bar)	Tensile Strength (MPa)	Impact Toughness (J)	Hardness (HRB)
1	120	90	3	1044.8	02.45	46.0
1	120	90	3	1078.4	02.42	48.2
1	120	90	3	1060.8	02.53	44.8
2	140	90	3	1083.2	03.61	52.4
2	140	90	3	1153.6	05.84	50.7
2	140	90	3	1137.6	03.93	50.2
3	120	120	3	1041.6	08.08	48.4
3	120	120	3	1142.4	07.19	48.2
3	120	120	3	1224.0	08.52	51.5
4	140	120	3	1364.8	17.43	56.2
4	140	120	3	1417.6	16.97	54.5
4	140	120	3	1384.0	17.80	56.1
5	120	90	7	1110.4	03.37	45.5
5	120	90	7	1177.6	03.10	49.2
5	120	90	7	1148.8	03.20	48.4
6	140	90	7	1212.8	05.20	52.9
6	140	90	7	1094.4	05.85	53.1
6	140	90	7	1048.0	05.86	55.4
7	120	120	7	1204.8	11.19	48.2
7	120	120	7	1345.6	11.00	49.5
7	120	120	7	1327.5	12.03	52.0
8	140	120	7	1446.4	16.40	59.1
8	140	120	7	1422.4	16.97	56.8
8	140	120	7	1432.0	16.19	60.8

Table A2 compares MRCC (non-optimal) curing parameters and non-optimum properties with optimal curing parameters and optimum properties.

Table A2. A comparative summary of non-optimum and optimum properties [28]

	Non-Optimal Curing Parameter	Non-Optimum Properties	Optimal Parameters	Optimum Properties	Improvement (%)
Tensile Strength (MPa)	120 °C 120 min 7 bar (MRCC/CC7)	1274.8	140 °C 120 min 7 bar (CC8)	1420	11.4
Impact Toughness (J)		10.9	140 °C 120 min 3 bar (CC4)	17.4	59.6
Hardness (HRB)		51.2	140 °C 120 min 7 bar (CC8)	57.6	12.5

Three Mathematical models of Previous Study

Equations (A1)–(A3) show the prediction model developed for tensile strength (*TS*), impact toughness (*IT*), and hardness (*HD*) of understudy CFRP.

$$TS = 2970 - 19.58T_c - 32.05t_c + 182P_{au} + 0.2979T_ct_c - 1.266T_cP_{au} \quad (A1)$$

$$IT = 180.6 - 2.098t_c - 1.575T_c - 23.98P_{au} + 0.01843T_ct_c + 0.18445T_cP_{au} + 0.2615P_{au}t_c - 0.00199T_cP_{au}t_c \quad (A2)$$

$$HD = -6.27 + 0.3263T_c + 0.1236t_c + 0.494P_{au} \quad (A3)$$

REFERENCES

1. Rajak, D.K.; Wagh, P.H.; Linul, E. Manufacturing Technologies of Carbon/Glass Fiber-Reinforced Polymer Composites and Their Properties: A Review. *Polymers (Basel).* **2021**, *13*, 3721, doi:10.3390/polym13213721.
2. Sreejith, M.; Rajeev, R.S. Fiber Reinforced Composites for Aerospace and Sports Applications. *Fiber Reinf. Compos.* 2021, 821–859.
3. Zhang, J.; Lin, G.; Vaidya, U.; Wang, H. Past, Present and Future Prospective of Global Carbon Fibre Composite Developments and Applications. *Compos. Part B Eng.* **2023**, *250*, 110463, doi:10.1016/j.compositesb.2022.110463 .
4. Stergiou, V.; Konstantopoulos, G.; Charitidis, C.A. Carbon Fiber Reinforced Plastics in Space: Life Cycle Assessment towards Improved Sustainability of Space Vehicles. *J. Compos. Sci.* **2022**, *6*, 144, doi:10.3390/jcs6050144.
5. Rubino, F.; Nisticò, A.; Tucci, F.; Carlone, P. Marine Application of Fiber Reinforced Composites: A Review. *J. Mar. Sci. Eng.* **2020**, *8*, 26, doi:10.3390/jmse8010026.
6. Almushaikeh, A.M.; Alaswad, S.O.; Alsuhybani, M.S.; AlOtaibi, B.M.; Alarifi, I.M.; Alqahtani, N.B.; Aldosari, S.M.; Alsaleh, S.S.; Haidyrah, A.S.; Alolyan, A.A.; et al. Manufacturing of Carbon Fiber Reinforced Thermoplastics and Its Recovery of Carbon Fiber: A Review. *Polym. Test.* **2023**, *122*, 108029, doi:10.1016/j.polymertesting.2023.108029.
7. Bhong, M.; Khan, T.K.H.; Devade, K.; Vijay Krishna, B.; Sura, S.; Eftikhaar, H.K.; Pal Thethi, H.; Gupta, N. Review of Composite Materials and Applications. *Mater. Today Proc.* **2023**, doi:10.1016/j.matpr.2023.10.026.
8. Gangineni, P.K.; Gupta K., B.N.V.S.G.; Patnaik, S.; Prusty, R.K.; Ray, B.C. Recent Advancements in Interface Engineering of Carbon Fiber Reinforced Polymer Composites and Their Durability Studies at Different Service Temperatures. *Polym. Compos.* **2022**, *43*, 4126–4164, doi:10.1002/pc.26716.
9. Boon, Y. Di; Joshi, S.C.; Bhudolia, S.K. Review: Filament Winding and Automated Fiber Placement with In Situ Consolidation for Fiber Reinforced Thermoplastic Polymer Composites. *Polymers (Basel).* **2021**, *13*, 1951, doi:10.3390/polym13121951.
10. Chen, Y.; Zhang, J.; Li, Z.; Zhang, H.; Chen, J.; Yang, W.; Yu, T.; Liu, W.; Li, Y. Manufacturing Technology of Lightweight Fiber-Reinforced Composite Structures in Aerospace: Current Situation and toward Intellectualization. *Aerospace* **2023**, *10*, 206, doi:10.3390/aerospace10030206.
11. Marrone, L. *Cure Path Dependency of Mode I Fracture Toughness of Recycled Aerospace-Grade Carbon Fibre Prepregs*; McGill University (Canada), 2022; ISBN 9798377674658.
12. Ekuase, O.A.; Anjum, N.; Eze, V.O.; Okoli, O.I. A Review on the Out-of-Autoclave Process for Composite Manufacturing. *J. Compos. Sci.* **2022**, *6*, 172, doi:10.3390/jcs6060172.

13. Butenegro, J.A.; Bahrami, M.; Martínez, M.Á.; Abenojar, J. Reuse of Carbon Fibers and a Mechanically Recycled CFRP as Rod-like Fillers for New Composites: Optimization and Process Development. *Processes* **2023**, *11*, 366, doi:10.3390/pr11020366.
14. Mathew, E.; Joshi, S.C. Effect of Roller Pressure and Base Prepreg Layer on Tensile and Flexural Properties of CFRP Laminates Fabricated Using Automated Fiber Placement. *J. Compos. Sci.* **2023**, *7*, 101, doi:10.3390/jcs7030101.
15. Feng, H.; Xu, X.; Wang, B.; Su, Y.; Liu, Y.; Zhang, C.; Zhu, J.; Ma, S. Facile Preparation, Closed-Loop Recycling of Multifunctional Carbon Fiber Reinforced Polymer Composites. *Compos. Part B Eng.* **2023**, *257*, 110677, doi:10.1016/j.compositesb.2023.110677.
16. Kumar, Y.; Sahoo, G. A Review on Gravitational Search Algorithm and Its Applications to Data Clustering & Classification. *Int. J. Intell. Syst. Appl.* **2014**, *6*, 79–93, doi:10.5815/ijisa.2014.06.09.
17. Goel, L. An Extensive Review of Computational Intelligence-Based Optimization Algorithms: Trends and Applications. *Soft Comput.* **2020**, *24*, 16519–16549, doi:10.1007/s00500-020-04958-w.
18. Devika, G.; Karegowda, A.G. Bio-Inspired Optimization: Algorithm, Analysis and Scope of Application. In *Swarm Intelligence-Recent Advances and Current Applications*; Aceves-Fernández, M.A., Ed.; IntechOpen, 2023; p. 196 ISBN 1837680876.
19. Rashedi, E.; Nezamabadi-pour, H.; Saryazdi, S. GSA: A Gravitational Search Algorithm. *Inf. Sci. (Ny).* **2009**, *179*, 2232–2248, doi:10.1016/j.ins.2009.03.004.
20. Hashemi, A.; Dowlatshahi, M.B.; Nezamabadi-Pour, H. Gravitational Search Algorithm: Theory, Literature Review, and Applications. *Handb. AI-based Metaheuristics* **2021**, 119–150.
21. Mittal, H.; Tripathi, A.; Pandey, A.C.; Pal, R. Gravitational Search Algorithm: A Comprehensive Analysis of Recent Variants. *Multimed. Tools Appl.* **2021**, *80*, 7581–7608.
22. Rashedi, E.; Rashedi, E.; Nezamabadi-pour, H. A Comprehensive Survey on Gravitational Search Algorithm. *Swarm Evol. Comput.* **2018**, *41*, 141–158, doi:10.1016/j.swevo.2018.02.018.
23. Zhang, N.; Li, C.; Li, R.; Lai, X.; Zhang, Y. A Mixed-Strategy Based Gravitational Search Algorithm for Parameter Identification of Hydraulic Turbine Governing System. *Knowledge-Based Syst.* **2016**, *109*, 218–237.
24. Deb, K. Multi-Objective Optimisation Using Evolutionary Algorithms: An Introduction. *Multi-objective Evol. Optim. Prod. Des. Manuf.* 2011, 3–34.
25. Harkare, V.; Mangrulkar, R.; Thorat, O.; Jain, S.R. Evolutionary Approaches for Multi-Objective Optimization and Pareto-Optimal Solution Selection in Data Analytics. In *Applied Multi-objective Optimization*; Springer, 2024; pp. 67–94.
26. Shehata, M.; Abdelnaeem, M.; Mokhiamar, O. Integrated Multiple Criteria Decision-Making Framework for Ranking Pareto Optimal Solutions of the Multiobjective Optimization Problem of Tuned Mass Dampers. *Ocean Eng.* **2023**, *278*, 114440.
27. Shandilya, S.K.; Datta, A.; Nagar, A.K. Nature-Inspired Algorithms. In *A Nature-Inspired Approach to Cryptology*; Springer, 2023; pp. 3–36.
28. Ahmad, F.; Awadh, M. Al; Abas, M.; Noor, S.; Hameed, A. Optimization of Carbon Fiber Reinforced Plastic Curing Parameters for Aerospace Application. *Appl. Sci.* **2022**, *12*, 4307.